Algae decorated TiO_2/Ag hybrid nanofiber membrane with enhanced photocatalytic activity for Cr(VI) removal under visible light

Lei Wang [a, 1], Changbo Zhang [b, 1], Feng Gao [c], Gilles Mailhot [d, e], Gang Pan[*a, f]

[a]Department of Environmental Nanotechnology, Research Center for Eco-environmental Sciences, Chinese Academy of Sciences,18 Shuangqing Road, Beijing 100085, P. R. China

[b]Agro-Environmental Protection Institute, Ministry of Agriculture, Tianjin 300191, China

[c]National Center for Nanoscience and Technology, 11 Zhongguancun Beiyitiao, Beijing 100190, P. R. China

[d]Clermont Université, Université Blaise Pascal, Institut de Chimie de Clermont-Ferrand (ICCF)-ENSCCF, BP 10448, F-63000 Clermont-Ferrand, France

[e]CNRS, UMR 6296, Institut de Chimie de Clermont-Ferrand, F-63171 Aubière, France

[f]School of Animal, Rural and Environmental Sciences, Nottingham Trent University, Brackenhurst Campus, Southwell NG25 0QF, United Kingdom

*Corresponding author

E-mail: gpan@rcees.ac.cn

[1]These authors should be regarded as co-first authors.

Abstract

Algae as an abundant natural biomass, more attention has been paid to explore its potential application in environmental pollutants treatment. This work prepared the algae-TiO_2/Ag bionano hybrid material by loading algae cells on the ultrafine TiO_2/Ag chitosan hybrid nanofiber mat. For the first time, the synergistic photocatalytic effect of fresh algae and TiO_2/Ag nanomaterial was investigated by removal of Cr(VI). The addition of algae significantly improved the photo-removal of Cr(VI) in the system with TiO_2/Ag hybrid nanomaterial under visible light irradiation. Meanwhile, the photocatalytic mechanism was studied. The photogenerated reactive oxygen species were quantified and the addition of algae apparently decreased the yields of •OH to 31.0 μM, while improved the yields of $^1O_2$ and $O_2^{\bullet-}$ in the reaction system with TiO_2/Ag hybrid nanofiber mats. The change of superoxide dismutase activity and malondialdehyde content in algae indicated that TiO_2/Ag could impose oxidative stress and cause lipid peroxidation in algae cells. During the course of irradiation, algae released substances could act as scavenger for holes, thus inhibited the recombination of hole/electron and enhanced the photocatalytic reduction of Cr(VI) by electrons on TiO_2 surface. Algae was simultaneously photodegraded in the system and the resulting $O_2^{\bullet-}$, organic free radicals could promote the reduction of Cr(VI). This functional hybrid nanofiber mat was easily recovered and maintained a great photocatalytic activity on the five successive cycles. This algae-photocatalyst hybrid material has promising applications potential in heavy metal removal and organic pollutants treatment.

Keywords: Photoreduction; Algae; TiO_2; Ag nanoparticles; hybrid nanofiber; Cr(VI)

1. Introduction

Cr(VI) is a common contaminant in waste water. The reduction of Cr(VI) to Cr(III) can reduce its toxicity and mobility in the environment [1]. Increasing attention has been paid to the TiO_2-mediated photocatalytic reduction [2-4]. However, its wide band gap (3.2 eV) limits the photocatalytic efficiency and practical application. Many methods have been adopted to improve TiO_2 photocatalytic efficiency [5, 6]. The metal-doped TiO_2 have attracted much attention. Introduction of metal ions can enhance the photocatalytic activity of TiO_2. TiO_2 with Ag nanoparticles act as electron trap, which enhance the electron-hole separation and facilitate interfacial electron transfer [7]. However, TiO_2 nanoparticles are hard to be recovered in the reaction solution and may cause secondary pollution. This drawback can be avoided by loading TiO_2 onto some supporting matrices [8-11]. When Cr(VI) alone was photocatalytic reduced in reaction solution, the reduction rate of Cr(VI) to Cr(III) proceeded quite slowly. If the reaction was paired with the photo-oxidation of organic compounds, such as salicylic acid, ethylene diamine tetraacetic acid (EDTA), the reduction rate of Cr(VI) was enhanced significantly, because the charge separation was enhanced by simultaneous reduction/oxidation reactions [12-14].

Algae is a wide spread microorganism in the natural environments. Algae can generate some smaller molecular weight organics, such as carboxylic groups (humic, fulvic acid, etc.) and phenolic hydroxyl groups. Algal photolysis is a possible alternative way for the degradation of aquatic environmental pollutants. In the

previous study, the photodegradation of organic and heavy metal pollutants could be accelerated by algae [15]. Algae cells could photogenerate reactive radicals that induced the degradation of pollutants [16]. Many reports demonstrated that TiO_2 nanoparticles were effective in deactivation and removal of harmful algae species [17-19], but few studies focused on the synergistic photocatalytic effect on the removal of pollutants by algae combined with TiO_2 or other nanocatalyst. The photocatalytic mechanism of algae-nanocatalyst hybrid material was unclear.

Moreover, microalgae application faces the same problem as TiO_2 powder, which is hard to be recovered from aqueous solution. Nanofiber membrane presents good matrix for immobilizing algae cells and TiO_2 catalysts due to its large specific surface area, high pore volume, uniform microporosity and high adsorption/desorption rate [20, 21]. As an abundant natural biomass, chitosan nanofibers are increasingly attracting more attention due to the structural advantages conveyed by the nanosized diameter of the constituent fibers [22-24]. Decreasing fiber diameter caused many beneficial effects, such as increased specific surface to volume ratios [25]. Although references have reported the generation of chitosan nanofibers, the preparation of large scale uniform ultrafine chitosan hybrid nanofiber in tens of nanometer is still a challenge.

This work aimed to fabricate the bionano hybrid material by loading algae cells (*Chlorella vulgaris*) on the ultrafine TiO_2/Ag chitosan hybrid nanofiber mats (TiO_2/Ag NF) and study the synergistic photocatalytic properties of algae-TiO_2/Ag nanofibers (algae-TiO_2/Ag NF) by removal of Cr(VI) under visible light. The

photogenerated reactive oxygen species (ROS) were quantified in different reaction systems with algae, pure TiO_2, TiO_2/Ag nanofibers and algae-TiO_2/Ag hybrid materials. The change of antioxidant enzymes activity in the algae cells were measured after irradiation. The synergistic photocatalytic mechanism of algae and TiO_2/Ag hybrid nanomaterial was investigated. So far, there is no study on the photocatalytic degradation of pollutants by the algae cells combined with the TiO_2/Ag hybrid nanofiber mats.

2. Material and Methods

2.1. Materials

Chitosan (B.R. grade, degree of deacetylation = 80.0-95.0%), Hydrochloric acid (37% of purity), Glutaraldehyde (GA) (50% in water), $K_2Cr_2O_7$, H_2SO_4, NaOH and Acetone were purchased from Sinopharm Chemical Reagent Co., Ltd. Silver nitrite ($AgNO_3$), sodium thiosulfate and acrylic acid (AA) were purchased from Beijing Chemical Works. KI, carbon tetrachloride (CCl_4), 2-propanol and benzoquinone were purchased from Aladdin (China). TiO_2 (anatase, particle size of 5-10 nm, specific surface area of 180 $m^2\ g^{-1}$) was purchased from Evonik Industries Metal Oxides. Polyvinyl alcohol (PVA) (typical MW of 118,000-124,000, 86–90% hydrolyzed) was obtained from Zhong Ke Guo Chang Technology Co., Ltd (Beijing, China). Nitroblue tetrazolium (NBT) was purchased from Wako Pure Chemical. All chemicals were used without further purification. The algae was purchased from the Wuhan Hydrobiology Institute of Chinese Academy of Sciences. Water with a conductivity of 18.2 MΩ cm at pH 7.0 was obtained from a Milli-Q system (Millipore Corp., Boston,

MA).

2.2. Preparation of algae decorated TiO_2/Ag chitosan hybrid nanofiber mat

Chitosan solution was prepared by dissolving 4.0 g of dry mass in 100 mL of 0.52 M acetic acid at room temperature, then heating to 60 °C with magnetic stirring for 24 h. PVA solutions were prepared by dissolving 10.0 g of PVA polymer in 100 mL deionized water at 60 °C, and completely dissolved by stirring. 0.5% of $AgNO_3$ and 1% of TiO_2 were well dispersed in the mixture with chitosan to PVA weight ratio 1/1 by mechanical stirring and ultrasonic treatment. The prepared mixed solutions were placed in a syringe (5 mL) with a metal capillary whose inner diameter is 0.57 mm. Electrospinning of nanofibers were performed at voltage of 30 kV (Spellman SL150), the tip-collector distance of 10 cm and the solution feed rate of 0.5 mL/h. The schematic diagram of electrospinning setup was shown in Fig. 1a. The electrospinning process by single needle electrospinning was shown in Fig. 1b. The randomly oriented nanofiber mat was collected on the aluminum foil and dried at room temperature in vacuum for 24 h.

The nanofiber mat can be easily separated from the aluminum foil and Fig. 1c shows the scale of part of nanofiber samples (30 cm × 20 cm). In order to improve their potential application in aqueous environment, the nanofibers were cross-linked by 4% GA solution. The algae-TiO_2/Ag NF was obtained by immerging TiO_2/Ag NF into the algae solution (exponential phase of growth) for 3 days to allow sufficient attachment of algae cells to the nanofiber mat (Fig. 1d).

2.3. Characterizations

The morphology and structure of nanofiber membranes were characterized by scanning electron microscopy (SEM, Hitachi S-4800, Japan), energy-dispersive X-ray spectroscopy (EDX, Horiba), transmission electron microscopy (TEM, Tecnai G2 20 ST, America) and X-ray diffraction (XRD, Regaku D/Max-2500 diffractometer equipped with a Cu $K\alpha_1$ radiation). The average fiber diameter was determined by the statistical treatment of SEM images with the image processing software Image J. The fiber diameter distribution was obtained by measuring at a minimum number of 50 nanofibers. Algae-TiO_2/Ag NF images were recorded by AFM Digital Instruments Dimension 3000 with a Nanoscope IIIa controller under contact mode, using silicon cantilevers.

2.4. Detection of reactive oxygen species

The photoproduction of reactive oxygen species (ROS) was determined in the reaction solution. Furfuryl alcohol (FFA) (1 mM) and benzene (1 mM) were used as probe to detect the singlet oxygen ($^1O_2$) and hydroxyl radical (•OH), respectively. [26] $^1O_2$ can be quantified by the loss of FFA. FFA was measured by high performance liquid chromatography (HPLC) (Agilent) with a C18 column (Agilent, 3.5 μm, 4.6 × 150 mm) at wavelength of 230 nm and the mobile phase was methanol and water (50:50, v/v) with a flow rate of 1.0 mL min^{-1}. It was recommended that •OH-mediated oxidation of benzene forms phenol with approximately 100% of yield and •OH concentration can be determined by the formation of phenol, which was measured by HPLC at 270 nm and the mobile phase was acetonitrile and water (40:60, v/v) with a flow rate of 0.8 mL min^{-1}. For the analysis of superoxide ion ($O_2^{\bullet-}$), experiment was

carried out in the solution with 1 mM of NBT and the amount of $O_2^{\bullet-}$ was quantified by detecting the decrease of NBT in the reaction solution (Shimadzu, UV2500) [27].

2.5. Measurement of lipid peroxidation and Chlorophyll-a

After 3 h of irradiation, algae cells were homogenized in the phosphate buffer solution (PBS, 4 °C, pH 7.8) by the ultrasonic cell pulverizer (Ningbo SCIENIZ, JY92-2D, China) in the ice bath and then centrifuged at 4000 rpm for 10 min at 4 °C. The malondialdehyde (MDA) content and superoxide dismutase (SOD) activity in algae cells were measured by reagent kit according to the instructions (Nanjing Jiancheng Biotechnology Institute, China) [28] and the used supernatant samples were 0.1 mL and 10 μL, respectively.

After 3 h of irradiation, Chlorophyll-a (Chl-a) of algae was extracted by acetone (90%) for 24 h at 4 °C in the dark. After 10 min of centrifugation at 3500 rpm, the supernatant of algae cell extract was tested at the wavelengths of 630, 645, 663 and 750 nm by a UV-vis spectrophotometer (Shimadzu, UV2500) and 90% of acetone was used as the control.

2.6. Photocatalytic reduction of Cr(VI)

Experiments were carried out in a home-made photochemical reactor with a 500 W halogen tungsten lamp with the major emission wavelengths above 400 nm (Shanghai Yaming Light, China) placed in a water jacket for maintaining a constant temperature at 25±2 °C by cooling water circulation. Light less than 400 nm was filtered with the cutoff filter (> 420 nm) to simulate visible light.

The stock solution of Cr(VI) was prepared by using analytical grade $K_2Cr_2O_7$. As

for photocatalytic reduction of Cr(VI), the obtained algae-TiO_2/Ag NF and TiO_2/Ag NF were investigated in 500 mL of Cr(VI) solution with different initial concentrations and pure TiO_2 system was set as control. The pH was adjusted with H_2SO_4 and NaOH. The reaction solution was further stirred in the dark for 60 min. During the photo-reaction, samples were collected at preset time intervals. In the pure TiO_2 reaction system, samples were centrifuged at 5000 rpm for 25 min. All of the samples were filtered through 0.22 μm filters and then the concentration of Cr(VI) was determined spectrophotometrically at 540 nm using diphenylcarbazide as the color agent by a UV-vis spectrophotometer (Shimadzu, UV2500). The photocatalytic reduction rate (R) of Cr(VI) was calculated by the following equation:

$$R= (1-C/C_0) \times 100\%$$

Where C_0 was the initial concentration of Cr(VI) and C was the concentration at various irradiation time.

In order to investigate the photocatalytic mechanism, active species trap experiments were conducted with different scavengers. KI (1 mM), CCl4 (1 mM), 2-propanol (1 mM) and benzoquinone (1 mM) were used as scavengers for trapping holes (h^+), electrons (e^-), hydroxyl radicals (•OH) and superoxide radical ($O_2^{\bullet-}$), respectively [29]. The experimental process was same to the photodegradation experiment. All the experiments were triplicate.

3. Results and Discussion

3.1. Preparation and characterization of algae-TiO_2/Ag hybrid nanofiber mat

As an abundant natural biomass, chitosan was used as the spinning materials in

this work. Chitosan nanofiber was not easily fabricated in the electrospinning process because of its native properties, such as low solubility, high degree of inter and intra-chain hydrogen bonding, and high solution viscosity [30]. The chitosan nanofibers always has a relatively greater diameter (hundreds of nm) and some bead structures. Herein, the chitosan/PVA polymer hybrid nanofibers with 0.5% $AgNO_3$ and 1% TiO_2 were fabricated by one step electrospinning method in this work. Fig. 2a shows the SEM image of TiO_2/Ag chitosan nanofiber mats after cross-linking by 4% GA solution. The obtained nanofiber remained the shape unaltered in the water environment. The average diameter of ultrafine nanofiber was about 36.7 nm (Fig. 2b). The addition of $AgNO_3$ and TiO_2 improved the conductivity of the spinning solution, thus obviously improving the electrospinning ability of the chitosan solution. TEM image showed that in situ formed Ag nanoparticles were well distributed on nanofibers and the average particles size was around 2.88 nm (Fig. 2c). In the XRD pattern of nanofibers containing pure TiO_2, these peaks appeared at 2θ values of 25.32, 48.06 and 53.97 were ascribed to diffraction peaks of anatase TiO_2 (101), (200) and (105) (Fig. 2d). TEM image of TiO_2/Ag NF showed that both nanoparticles were anchored on the nanofibers (Fig. 2e). Ag and TiO_2 deposition were further verified by energy dispersive X-ray spectroscopy analysis (Fig. 2f). The addition of Ag and TiO_2 could help improve the function of hybrid nanofibers, such as catalysis and antibacterial activity [31, 32].

The obtained hybrid nanofiber membrane was employed as a support matrix for green algae (*Chlorella vulgaris*) in this study. Fig. 3a showed the optical image of

algae decorated nanofiber membrane and the green color indicated the attachment of algae cells on the surface of hybrid nanofiber mats. This was attributed to the electrostatic attraction between algae cells with negative surface charge and chitosan with positive charge primary amine group. As shown in Fig. 4, the height profile of nanofiber mats before and after loading algae were characterized by AFM, and the thickness of algae layer was about 2.5-3 μm close to the size of algae cell, which indicated a single layer of algae attached on the surface of nanofibers. The detailed structure was characterized by SEM and algae cells were well dispersed on the surface of the nanofiber mats with density of 5 cells per 100 μm^2 after 3 days (Fig. 3b-c). The hybrid nanofibers remained their shape after a long time contact with water and the ultrafine nanofibers with high specific surface area became an effective support matrix for algae.

3.2. Photoproduction of ROS

The photogenerated ROS was analyzed in different reaction systems with algae, pure TiO_2, TiO_2/Ag NF and algae-TiO_2/Ag NF, respectively. Fig. 5 showed that algae cells could generate ROS under visible light irradiation. After 3 h irradiation, the yields of $^1O_2$ and $O_2^{\bullet-}$ were achieved 37.5 μM and 20.0 μM, respectively, which were much higher than that of •OH 4.0 μM. Chlorophyll was proved with photosensitizer property to generate ROS [33]. In this study, the Chl-a content was decreased from 0.28 to 0.10 mg/m^3 in system with algae after 3 h irradiation (Fig. 6).

From Fig. 5, •OH and $O_2^{\bullet-}$ were major active species photogenerated in the TiO_2/Ag NF or TiO_2 reaction systems. It was obviously that TiO_2/Ag NF presented

high photocatalytic activity under visible light, after 3 h irradiation, the yields of •OH and $O_2^{\bullet-}$ reached 72.0 μM and 7.9 μM, respectively, which were much higher than that in the aqueous solution with only TiO_2. The electron–hole pairs generated by TiO_2 under the excitation of UV can effectively reduce or oxidize species in solution to form ROS, while this process was negligible under visible light irradiation. Ag was demonstrated effective in improving photocatalytic activity of TiO_2 nanomaterial under visible light, which could be attributed to its higher light absorption characteristics in visible regions, separation efficiency of electron–hole and plasmon resonance effect [34].

The photochemical process of algae-TiO_2/Ag hybrid material was investigated. Results demonstrated that the addition of algae apparently decreased the yields of •OH to 31.0 μM. However, the generation rates of $^1O_2$ and $O_2^{\bullet-}$ were increased compared with that in the system with algae, TiO_2 or TiO_2/Ag NF. The previous research demonstrated that algae cells were gradually destroyed under irradiation and resulted in the release of intracellular substances, including carboxylic acids, carbohydrates, chlorophylls and amino acids [35]. The TiO_2/Ag material intensified the damage process of algae cells due to the efficient photocatalytic properties (Fig. 7). After 3 h irradiation, the Chl-a content was decreased from 0.28 to 0.03 mg/m^3 and about 90% of Chl-a was photodegraded in the presence of TiO_2/Ag NF (Fig. 6). Thus, the damaged algae cells could consume ROS and resulted in the decrease of •OH yields in the system. Meanwhile, the released intracellular substances (carboxylic acids, chlorophyll) could further promote the photo-production of $^1O_2$ and $O_2^{\bullet-}$. The

photogenerated $O_2^{\bullet-}$ and organic free radicals could simultaneously induce the reduction process.

The SOD activity and MDA content in the algae cells were measured after 3 h irradiation. As shown in Fig. 6b, the SOD activity was inhibited under irradiation and it was decreased significantly in the presence of TiO_2/Ag NF compared with that of the control. Meanwhile, the MDA content was significantly increased after irradiation (Fig. 6c). The MDA content of the algae cell in the TiO_2/Ag NF photocatalytic reaction system was 2.0 fold higher than that of the irradiation treatment, indicating that TiO_2/Ag NF could impose oxidative stress and cause lipid peroxidation in algae. Therefore, more intracellular substances can be released and consume the holes and highly oxidative radicals.

3.3. Photocatalytic reduction of Cr(VI)

Before irradiation experiment, the absorption properties of the TiO_2/Ag NF and algae-TiO_2/Ag NF were investigated respectively. From Fig. 8a, the TiO_2/Ag NF could absorb 6% of Cr(VI) in 3 h dark experiment. It was mainly because chitosan could form complexes with metal ions by amino groups and TiO_2 could absorb some anionic chromate species ($HCrO_4^-$ and/or $Cr_2O_7^{2-}$) by the strong electrostatic attraction. While the algae-TiO_2/Ag NF could absorb 11% of Cr(VI). This improvement was attributed to the absorption ability of algae cells that mainly contain polysaccharides and lipids, which offered many functional groups to sequester more metal ions [36]. However, absorption was not a priority method when the removal efficiency was considered in reducing the toxicity and reduction of the pollutants. Photocatalytic

experiments were performed under visible light in various systems with TiO_2/Ag NF and algae-TiO_2/Ag NF, and pure TiO_2 was set as control. From Fig. 8a, TiO_2 exhibited negligible photoreduction rate of Cr(VI) under visible light irradiation, while the TiO_2/Ag NF was photoactive in the reduction of Cr(VI). The addition of Ag was an effective strategy for narrowing the band gap and improving the photocatalytic activity of TiO_2 under visible light irradiation. Furthermore, the TiO_2/Ag NF can be easily recovered from the solution after reaction. The addition of algae cells significantly increased the photocatalytic reduction rate of Cr(VI). After 3 h reaction, above 50% of Cr(VI) was removed in the system with algae-TiO_2/Ag NF. Effect of initial Cr(VI) concentration on the reaction was examined in the presence of algae-TiO_2/Ag NF at pH 4.0 with different initial concentrations of Cr(VI) at 5.0, 10.0, 30.0, 50.0 and 100.0 mg L^{-1}, respectively. From Fig. 8b, the algae-TiO_2/Ag NF was effect in the removal of Cr(VI) at various concentrations, but the higher the initial Cr(VI) concentration, the lower Cr(VI) photodegradation efficiency was. Large amount of Cr(VI) ions in aqueous solution could compete active sites on the algae-TiO_2/Ag NF and caused low reduction rate of Cr(VI) with high initial concentration.

Fig. 8c exhibited the influence of pH on the photocatalytic process. It was apparently that the acid medium facilitated the photocatalytic reduction of Cr(VI). A photoreduction rate of 91%, 80%, 50%, 40% and 25% was achieved in the presence of algae-TiO_2/Ag NF at pH 2.0, 3.0, 4.0, 6.0 and 8.0, respectively. The pH effect was caused by the formation of different Cr(VI) species. H_2CrO_4 was the dominant species

at pH less than 2.0, $HCrO_4^-$ at pH 2.0-5.0, $Cr_2O_7^{2-}$ ions at pH 5.0-7.0 and CrO_4^{2-} was predominant in alkaline medium [37]. Redox potential of $HCrO_4^-$ was higher than that of CrO_4^{2-} and easy to be reduced in the system with algae-TiO_2/Ag NF. pH can affect the surface charge of TiO_2, with decreasing the pH value, the surface of TiO_2 can be more positively charged, which improving the adsorption ability of $HCrO_4^-$ onto the TiO_2 surface and leading to the increase of photocatalytic reduction rate of Cr(VI).

3.4. Photoreduction mechanism of Cr(VI)

For investigation of the photoreduction mechanism, active species trapping experiments were performed by using different individual scavengers. KI, CCl4, 2-propanol and benzoquinone were used as scavengers for trapping holes, electrons, •OH and $O_2^{\bullet-}$, respectively. From Fig. 9, when CCl_4 or benzoquinone was added in the system, the photoreduction of Cr(VI) was inhibited compared with that without scavengers. It could be concluded that electron and $O_2^{\bullet-}$ were main active species in Cr(VI) reduction. While the addition of KI or 2-propanol showed a small positive effect on the removal of Cr(VI). This slight increasing indicated that the trap of holes decreased the opportunity to recombine electron–hole pairs, facilitating the generation of more electrons.

The proposed mechanism of Cr(VI) removal was shown in Fig. 10. The Ag nanoparticles could capture the photogenerated electrons and prolong the lifetime of charge carriers due to the surface plasmon resonance effect, thus leading to the promoted photocatalytic activity of TiO_2 under visible light [38]. Herein, the TiO_2/Ag NF significantly increased the algae cell damage process. Algae cells contain a large

quantity of glycoprotein, hydroxyproline, polysaccharides and lipids [39]. During the irradiation process, algae cell gave off dissolved organic matter, such as carboxylic groups and phenolic hydroxyl groups. The oxidation of these algae substances could consume photo-excited holes and •OH efficiently, which attenuated the electron–hole recombination and enhanced the photocatalytic reduction of Cr(VI) on TiO_2 surface. Algae photolysis was another pathway to remove Cr(VI). Irradiation of algae chlorophylls was able to absorb photons, which increased the yields of $O_2^{\bullet-}$ and organic radicals to accelerate the reduction of Cr(VI) (Fig. 5). Algae cells were simultaneously photodegraded in the reaction system. The released carboxylate acids could from complex with Cr(VI) and the generated organic free radicals could also react with Cr(VI), thus resulting in the efficient photoreduction of Cr(VI).

3.5. Repeated tests

Due to pollutants adsorption on active sites and fouling, to investigate the possible deactivation of catalysts, photocatalytic experiments were performed repeatedly for five times by recovering the used nanofibers. From the results of these repeated tests (Fig. 11), the activity of algae-TiO_2/Ag NF decreased by about 10% after five recycling tests. It was mainly attributed to pollutants irreversible absorption and the loss of active spots. Although slight decrements in photocatalytic activity were observed, the algae-TiO_2/Ag NF still maintained a high level of activity in successive cycles. A similar phenomenon was found in photo-transformation of aniline and benzo[a]pyrene by algae cells, and the photolysis of pollutants were still efficient in the presence of dead algae cells [26, 40]. This finding confirmed that algae-TiO_2/Ag

NF was stable and effective for the reduction of Cr(VI) and could be easily recovered based on its good settling properties.

4. Conclusions

This work fabricated the algae-TiO_2/Ag bionano hybrid materials that were composed of microalgae and ultrafine water-insoluble TiO_2/Ag hybrid nanofiber mats. The addition of algae significantly improved the photocatalytic activity of TiO_2/Ag NF on the removal of Cr(VI) under visible light. The synergy photocatalytic mechanism of algae and TiO_2/Ag hybrid nanomaterial was discussed in the present work. Algae released organic substances consumed photo-excited holes and •OH efficiently, which attenuated the electron–hole recombination and enhanced the photocatalytic reduction of Cr(VI) on TiO_2. Meanwhile, the release intracellular substance (chlorophylls, carboxylate acids) could be served as photosensitizers to improve the generation of $O_2^{\bullet-}$ and organic free radicals, which enhanced the photoreduction of Cr(VI) in the system. The bionano hybrid materials maintained a high activity in the five successive cycles and easy to be removed from the solution. These results gave an enlightenment to employ this bionano hybrid materials to remove organic/inorganic pollutants from waste water under irradiation, although further research will be needed before these approaches could be successfully applied in industrial and/or municipal wastewater treatment processes.

Acknowledgements

This work was supported by National Natural Science Foundation of China (21407160, 21107055), Natural Science Funds Fund form Tianjin

(13JCYBJC20300), Strategic Priority Research Program of the Chinese Academy of Sciences (XDA09030203) and the Science Promotion Programme of Research Center for Eco-environmental Sciences, CAS (YSW2013B05).

References

[1] C.E. Barrera-Diaz, V. Lugo-Lugo, B. Bilyeu, A review of chemical, electrochemical and biological methods for aqueous Cr(VI) reduction, J. Hazard. Mater. 223 (2012) 1-12.

[2] R. Qiu, D. Zhang, Z. Diao, X. Huang, C. He, J.L. Morel, Y. Xiong, Visible light induced photocatalytic reduction of Cr(VI) over polymer-sensitized TiO_2 and its synergism with phenol oxidation, Water Res. 46 (2012) 2299-2306.

[3] Y. Yang, G. Wang, Q. Deng, D.H.L. Ng, H. Zhao, Microwave-assisted fabrication of nanoparticulate TiO_2 microspheres for synergistic photocatalytic removal of Cr(VI) and methyl orange, Acs Appl. Mater. Inter. 6 (2014) 3008-3015.

[4] Y. Kim, H. Joo, N. Her, Y. Yoon, C.-H. Lee, J. Yoon, Self-rotating photocatalytic system for aqueous Cr(VI) reduction on TiO_2 nanotube/Ti mesh substrate, Chem. Eng. J. 229 (2013) 66-71.

[5] S.C. Xu, S.S. Pan, Y. Xu, Y.Y. Luo, Y.X. Zhang, G.H. Li, Efficient removal of Cr(VI) from wastewater under sunlight by Fe(II)-doped TiO_2 spherical shell, J. Hazard. Mater. 283 (2015) 7-13.

[6] L. Yang, Y. Xiao, S. Liu, Y. Li, Q. Cai, S. Luo, G. Zeng, Photocatalytic reduction of Cr(VI) on WO_3 doped long TiO_2 nanotube arrays in the presence of citric acid, Appl. Catal. B-Environ. 94 (2010) 142-149.

[7] P. Zhang, C. Shao, Z. Zhang, M. Zhang, J. Mu, Z. Guo, Y. Sun, Y. Liu, Core/shell nanofibers of TiO_2@carbon embedded by Ag nanoparticles with enhanced visible photocatalytic activity, J. Mater. Chem. 21 (2011) 17746-17753.

[8] L.W. Zhang, H.B. Fu, Y.F. Zhu, Efficient TiO_2 photocatalysts from surface hybridization of TiO_2 particles with graphite-like carbon, Adv. Funct. Mater. 18 (2008) 2180-2189.

[9] X. Zheng, D. Chen, z. Wang, Y. Lei, R. Cheng, Nano-TiO_2 membrane adsorption reactor (MAR) for virus removal in drinking water, Chem. Eng. J. 230 (2013) 180-187.

[10] E. Bet-moushoul, Y. Mansourpanah, K. Farhadi, M. Tabatabaei, TiO_2 nanocomposite based polymeric membranes: A review on performance improvement for various applications in chemical engineering processes, Chem. Eng. J. 283 (2016) 29-46.

[11] M.S. Jyothi, V. Nayak, M. Padaki, R.G. Balakrishna, K. Soontarapa, Aminated polysulfone/TiO_2 composite membranes for an effective removal of Cr(VI), Chem. Eng. J. 283 (2016) 1494-1505.

[12] G. Kim, W. Choi, Charge-transfer surface complex of EDTA-TiO_2 and its effect on photocatalysis under visible light, Appl. Catal. B-Environ. 100 (2010) 77-83.

[13] N. Wang, L. Zhu, K. Deng, Y. She, Y. Yu, H. Tang, Visible light photocatalytic reduction of Cr(VI) on TiO_2 in situ modified with small molecular weight organic acids, Appl. Catal. B-Environ. 95 (2010) 400-407.

[14] L. Wang, N. Wang, L. Zhu, H. Yu, H. Tang, Photocatalytic reduction of Cr(VI) over different TiO_2 photocatalysts and the effects of dissolved organic species, J. Hazard. Mater. 152 (2008) 93-99.

[15] L. Deng, F. Wu, N. Deng, Y. Zuo, Photoreduction of mercury(II) in the presence of algae, Anabaena cylindrical, J. Photoch. Photobio. B 91 (2008) 117-124.

[16] X.L. Liu, F. Wu, N. Deng, Photoproduction of hydroxyl radicals in aqueous solution with algae

under high-pressure mercury lamp, Environ. Sci. Technol. 38 (2004) 296-299.
[17] V. Rodriguez-Gonzalez, S.O. Alfaro, L.M. Torres-Martinez, S.H. Cho, S.W. Lee, Silver-TiO_2 nanocomposites: Synthesis and harmful algae bloom UV-photoelimination, Appl. Catal. B-Environ. 98 (2010) 229-234.
[18] B. Xia, B. Chen, X. Sun, K. Qu, F. Ma, M. Du, Interaction of TiO_2 nanoparticles with the marine microalga *Nitzschia closterium*: Growth inhibition, oxidative stress and internalization, Sci. Total Environ. 508 (2015) 525-533.
[19] J. Ji, Z. Long, D. Lin, Toxicity of oxide nanoparticles to the green algae Chlorella sp, Chem. Eng. J. 170 (2011) 525-530.
[20] E. Eroglu, V. Agarwal, M. Bradshaw, X. Chen, S.M. Smith, C.L. Raston, K.S. Iyer, Nitrate removal from liquid effluents using microalgae immobilized on chitosan nanofiber mats, Green Chem. 14 (2012) 2682-2685.
[21] X. Zhang, D.K. Wang, D.R.S. Lopez, J.C. Diniz da Costa, Fabrication of nanostructured TiO_2 hollow fiber photocatalytic membrane and application for wastewater treatment, Chem. Eng. J. 236 (2014) 314-322.
[22] J.D. Schiffman, C.L. Schauer, A review: electrospinning of biopolymer nanofibers and their applications, Polym. Rev. 48 (2008) 317-352.
[23] F. Ding, H. Deng, Y. Du, X. Shi, Q. Wang, Emerging chitin and chitosan nanofibrous materials for biomedical applications, Nanoscale 6 (2014) 9477-9493.
[24] H. Deng, P. Lin, S. Xin, R. Huang, W. Li, Y. Du, X. Zhou, J. Yang, Quaternized chitosan-layered silicate intercalated composites based nanofibrous mats and their antibacterial activity, Carbohyd. Polym. 89 (2012) 307-313.
[25] V. Sencadas, D.M. Correia, A. Areias, G. Botelho, A.M. Fonseca, I.C. Neves, J.L.G. Ribelles, S.L. Mendez, Determination of the parameters affecting electrospun chitosan fiber size distribution and morphology, Carbohyd. Polym. 87 (2012) 1295-1301.
[26] L. Wang, C. Zhang, F. Wu, N. Deng, Photodegradation of aniline in aqueous suspensions of microalgae, J. Photoch. Photobio. B 87 (2007) 49-57.
[27] H. Goto, Y. Hanada, T. Ohno, M. Matsumura, Quantitative analysis of superoxide ion and hydrogen peroxide produced from molecular oxygen on photoirradiated TiO_2 particles, J. Catal. 225 (2004) 223-229.
[28] X. Deng, F. Wu, Z. Liu, M. Luo, L. Li, Q. Ni, Z. Jiao, M. Wu, Y. Liu, The splenic toxicity of water soluble multi-walled carbon nanotubes in mice, Carbon 47 (2009) 1421-1428.
[29] L. Cai, X.L. Xiong, N.G. Liang, Q.Y. Long, Highly effective and stable Ag_3PO_4-WO_3/MWCNTs photocatalysts for simultaneous Cr(VI) reduction and orange II degradation under visible light irradiation, Applied Surface Science 353 (2015) 939-948.
[30] Y. Zhou, D. Yang, J. Nie, Electrospinning of chitosan/poly(vinyl alcohol)/acrylic acid aqueous solutions, J. Appl. Polym. Sci. 102 (2006) 5692-5697.
[31] E. Navarro, F. Piccapietra, B. Wagner, F. Marconi, R. Kaegi, N. Odzak, L. Sigg, R. Behra, Toxicity of silver nanoparticles to chlamydomonas reinhardtii, Environ. Sci. Technol. 42 (2008) 8959-8964.
[32] C.N. Lok, C.M. Ho, R. Chen, Q.Y. He, W.Y. Yu, H.z. Sun, P.K.H. Tam, J.F. Chiu, C.M. Che, Silver nanoparticles: partial oxidation and antibacterial activities, J. Biol. Inorg. Chem. 12 (2007) 527-534.
[33] F. Li, Z. Liang, X. Zheng, W. Zhao, M. Wu, Z. Wang, Toxicity of nano-TiO_2 on algae and the site of reactive oxygen species production, Aquat. Toxicol. 158 (2015) 1-13.
[34] J.F. Guo, B.W. Ma, A.Y. Yin, K.N. Fan, W.L. Dai, Highly stable and efficient Ag/AgCl@TiO_2

photocatalyst: Preparation, characterization, and application in the treatment of aqueous hazardous pollutants, J. Hazard. Mater. 211 (2012) 77-82.
[35] Z.e. Peng, F. Wu, N. Deng, Photodegradation of bisphenol A in simulated lake water containing algae, humic acid and ferric ions, Environ. Pollut. 144 (2006) 840-846.
[36] Z.R. Holan, B. Volesky, I. Prasetyo, Biosorption of cadmium by biomass of marine algae, Biotechnol. Bioeng. 41 (1993) 819-825.
[37] L. Deng, H. Wang, N. Deng, Photoreduction of chromium(VI) in the presence of algae, Chlorella vulgaris, J. Hazard. Mater. 138 (2006) 288-292.
[38] X.F. Lei, X.X. Xue, H. Yang, Preparation and characterization of Ag-doped TiO_2 nanomaterials and their photocatalytic reduction of Cr(VI) under visible light, Appl. Surf. Sci. 321 (2014) 396-403.
[39] R.H. Crist, K. Oberholser, N. Shank, M. Nguyen, Nature of bonding between metallic ions and algal cell walls, Environ. Sci. Technol. 15 (1981) 1212-1217.
[40] L. Luo, X. Lai, B. Chen, L. Lin, L. Fang, N.F.Y. Tam, T. Luan, Chlorophyll catalyse the photo-transformation of carcinogenic benzo a pyrene in water, Sci. Rep-UK 5 (2015) 12776.

Figure captions

Fig. 1 (a) schematic diagram of electrospinning setup, (b) generation process of nanofibers by single needle electrospinning, (c) optical image of large scale nanofibers mat and (d) diagram illustrating the preparation of algae decorated TiO_2/Ag hybrid nanofiber membrane

Fig. 2 (a) Fe-SEM image of TiO_2/Ag chitosan nanofiber mats cross-linked by 4% GA solution, (b) diameter distribution of nanofibers, (c) TEM image of nanofiber containing Ag, (d) XRD pattern of TiO_2 NF, (e) TEM image of TiO_2/Ag NF and (f) EDX spectra of hybrid nanofibers

Fig. 3 Optical image of algae-decorated nanofiber membrane (a) and SEM images of *Chlorella vulgaris* on the surface of TiO_2/Ag NF at (b) high and (c) low magnification

Fig. 4 AFM images of TiO_2/Ag NF before and after loading *Chlorella vulgaris* cells

Fig. 5 Photo-production of reactive oxygen species (a) •OH, (b) $^1O_2$ and (c) $O_2^{\bullet-}$ in aqueous solution. The density of free algae cells was 1.0×10^7 cells L^{-1}, which was the same as the attached cells number; the TiO_2/Ag NF was 1.0 g L^{-1}, the TiO_2 concentration was 10.0 mg L^{-1} and pH was 4.0

Fig. 6 Chl-a, SOD activity and MDA content of algae in different systems (a) pure algae, (b) algae with irradiation and (c) algae-TiO_2/Ag NF with irradiation

Fig. 7 SEM images of photo-damaged algae cells on the surface of TiO_2/Ag NF at (a) high and (b) low magnification

Fig. 8 (a) Photoreduction of Cr(VI) in different system with initial concentration of Cr(VI) = 10.0 mg L^{-1}, pH = 4.0; (b) different initial concentration of Cr(VI) and (c)

pH effects on the photoreduction of Cr(VI) in the system with algae-TiO_2/Ag NF

Fig. 9 Active species trapping experiments for the degradation of Cr(VI)

Fig. 10 Schematic of Cr(VI) photoreduction by algae-TiO_2/Ag hybrid nanofiber mat

Fig. 11 Repeated test for the photoreduction of Cr(VI) (10.0 mg L^{-1}, pH = 4.0)

Fig. 1

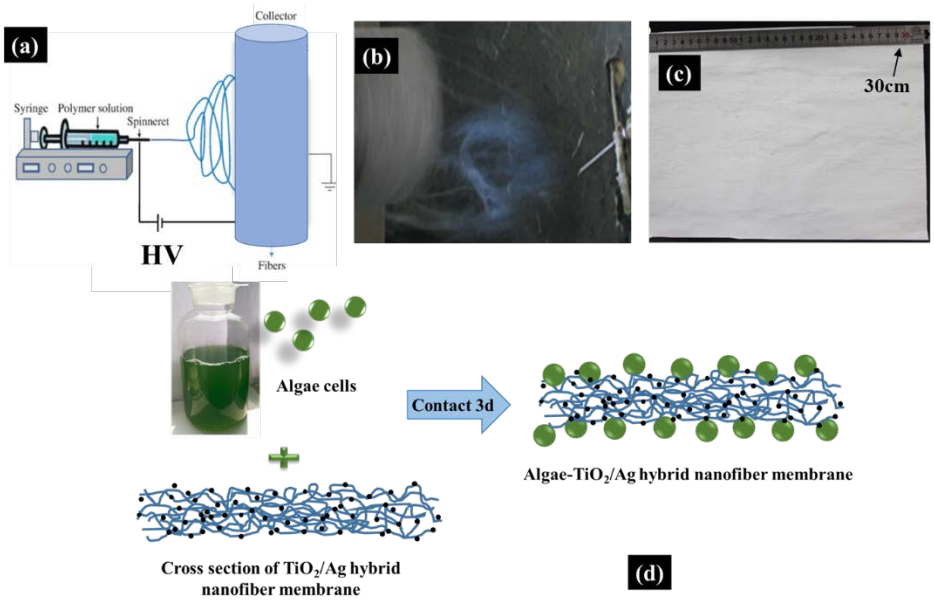
(a)
Collector
Syringe
Polymer solution
Spinneret
HV
Fibers
(b)
(c)
30cm
Algae cells
Contact 3d
Algae-TiO2/Ag hybrid nanofiber membrane
Cross section of TiO2/Ag hybrid nanofiber membrane
(d)

Fig. 2

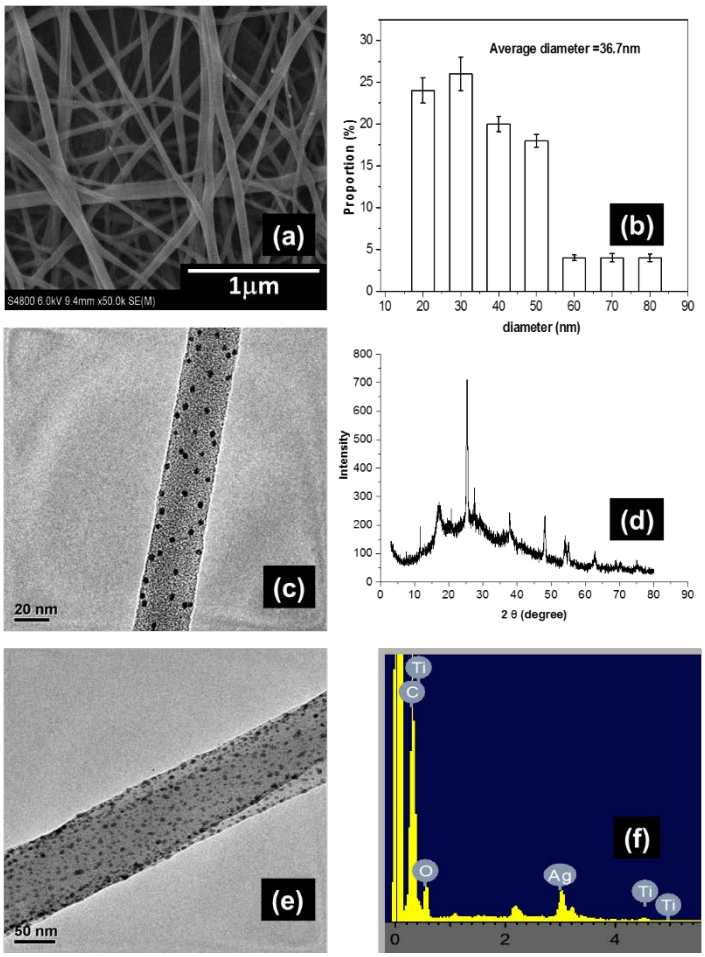
(a)
1μm
S4800 6.0kV 9.4mm x50.0k SE(M)
Average diameter =36.7nm
Proportion (%)
diameter (nm)
(b)
(c)
20 nm
Intensity
2 θ (degree)
(d)
(e)
50 nm
Ti
C
O
Ag
Ti
Ti
(f)

Fig. 3

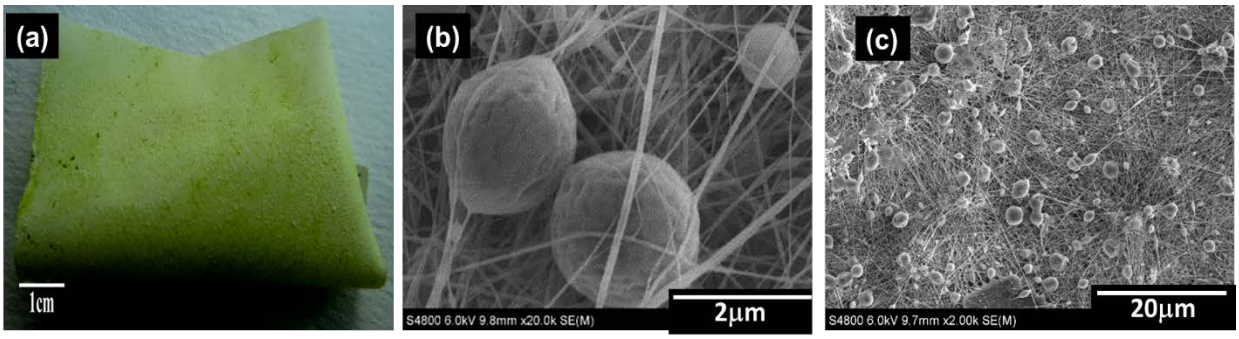
(a)
1cm
(b)
S4800 6.0kV 9.8mm x20.0k SE(M)
2μm
(c)
S4800 6.0kV 9.7mm x2.00k SE(M)
20μm

Fig. 4

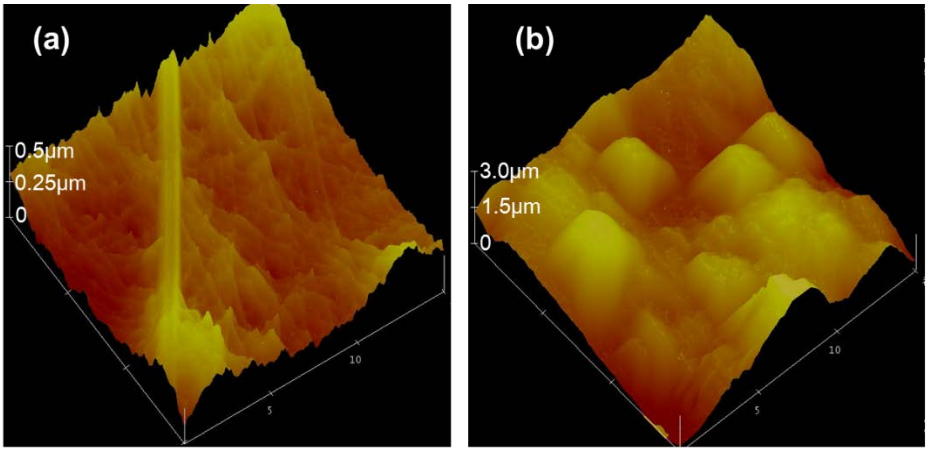

Fig. 5

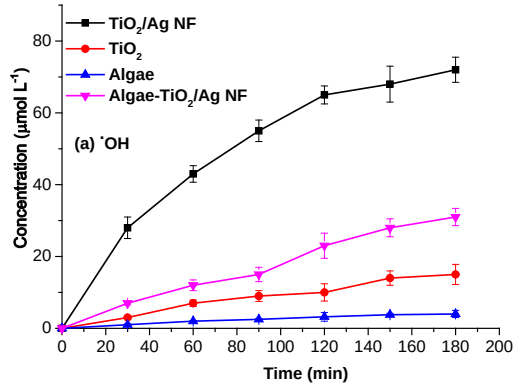
TiO2/Ag NF
TiO2
Algae
Algae-TiO2/Ag NF
(a) ˙OH
Concentration (µmol L-1)
Time (min)

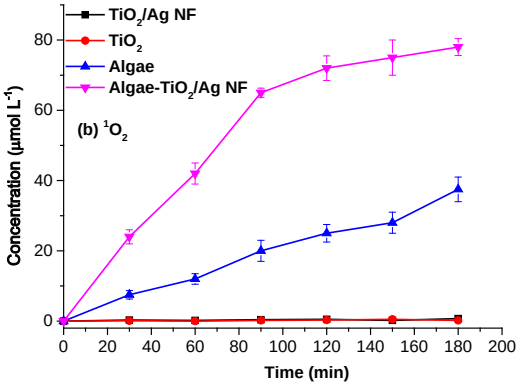
TiO2/Ag NF
TiO2
Algae
Algae-TiO2/Ag NF
(b) 1O2
Concentration (µmol L-1)
Time (min)

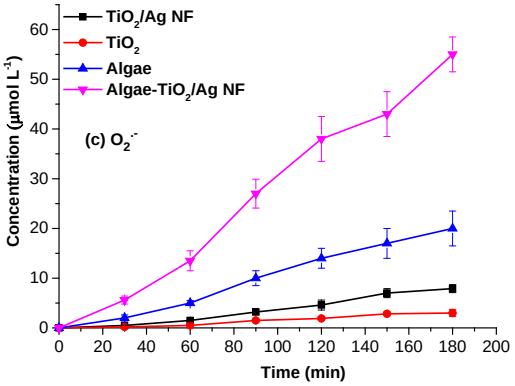
TiO2/Ag NF
TiO2
Algae
Algae-TiO2/Ag NF
(c) O2˙-
Concentration (µmol L-1)
Time (min)

Fig. 6

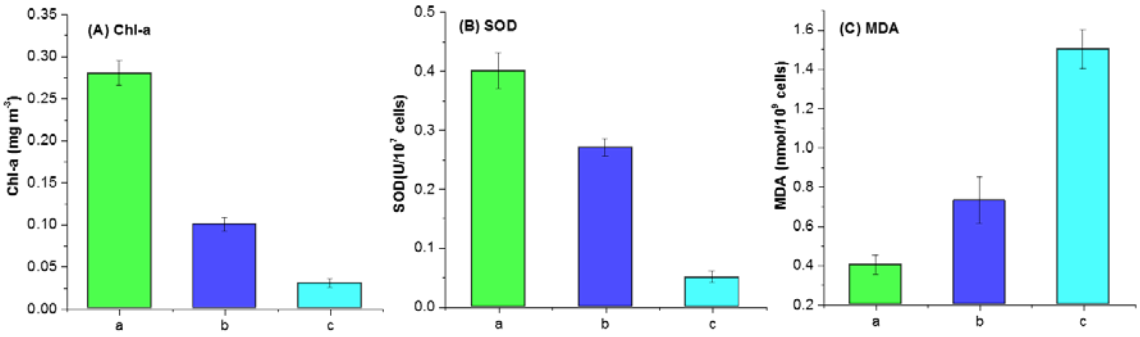
(A) Chl-a
Chl-a (mg m^{-3})
0.35
0.30
0.25
0.20
0.15
0.10
0.05
0.00
a
b
c
(B) SOD
SOD(U/10^{7} cells)
0.5
0.4
0.3
0.2
0.1
0.0
a
b
c
(C) MDA
MDA (nmol/10^{6} cells)
1.6
1.4
1.2
1.0
0.8
0.6
0.4
0.2
a
b
c

Fig. 7

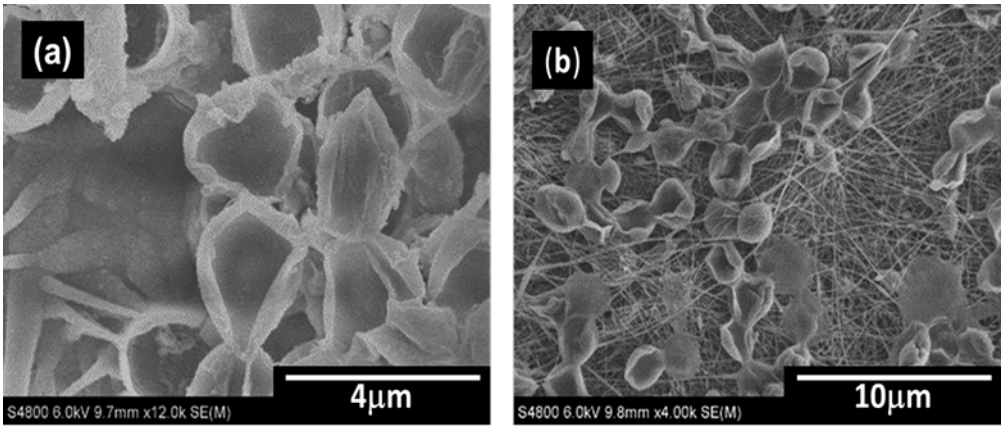
(a)
4μm
S4800 6.0kV 9.7mm x12.0k SE(M)
(b)
10μm
S4800 6.0kV 9.8mm x4.00k SE(M)

Fig.8

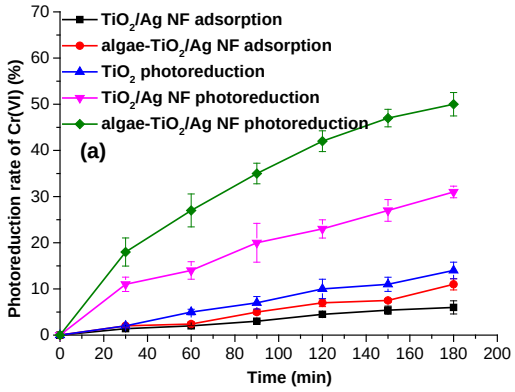
TiO2/Ag NF adsorption
algae-TiO2/Ag NF adsorption
TiO2 photoreduction
TiO2/Ag NF photoreduction
algae-TiO2/Ag NF photoreduction
(a)
Photoreduction rate of Cr(VI) (%)
Time (min)

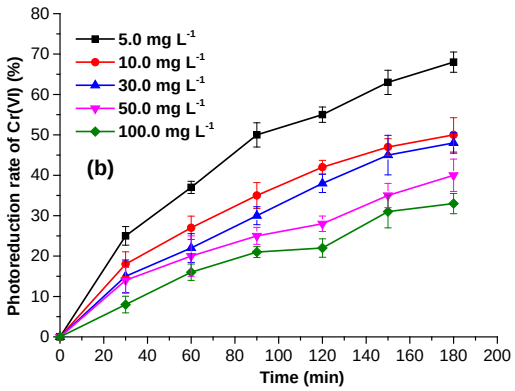
5.0 mg L-1
10.0 mg L-1
30.0 mg L-1
50.0 mg L-1
100.0 mg L-1
(b)
Photoreduction rate of Cr(VI) (%)
Time (min)

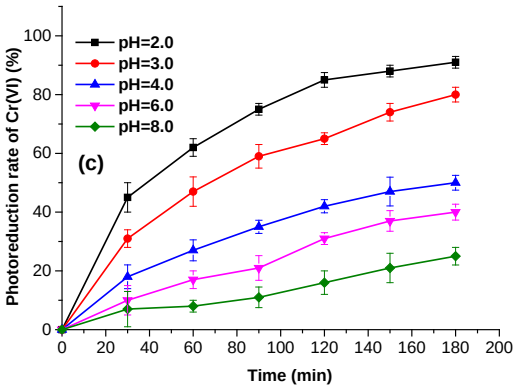
pH=2.0
pH=3.0
pH=4.0
pH=6.0
pH=8.0
(c)
Photoreduction rate of Cr(VI) (%)
Time (min)

Fig. 9

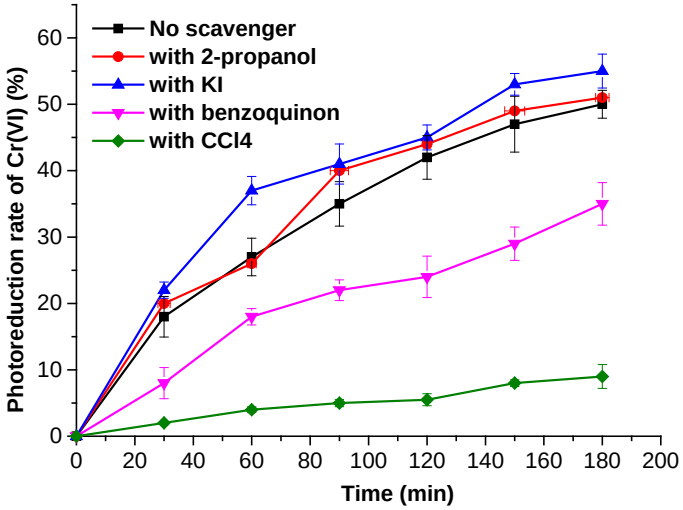
No scavenger
with 2-propanol
with KI
with benzoquinon
with CCl4
Photoreduction rate of Cr(VI) (%)
Time (min)
0
10
20
30
40
50
60
0
20
40
60
80
100
120
140
160
180
200

Fig. 10

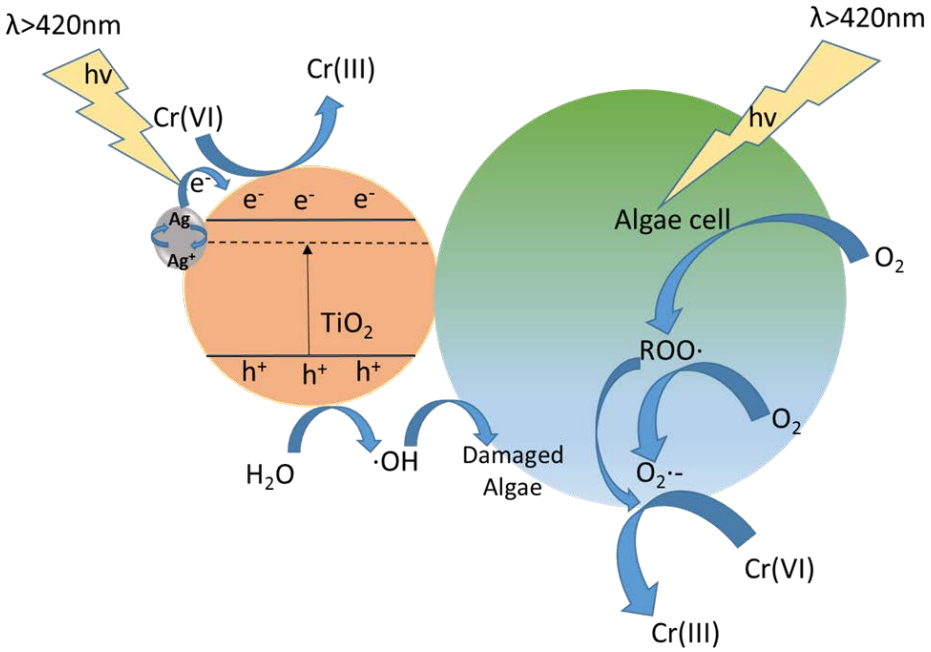
λ>420nm
hv
Cr(VI)
Cr(III)
e⁻
e⁻ e⁻ e⁻
Ag
Ag⁺
TiO2
h⁺ h⁺ h⁺
H2O
·OH
Damaged Algae
λ>420nm
hv
Algae cell
O2
ROO·
O2
O2·-
Cr(VI)
Cr(III)

Fig. 11

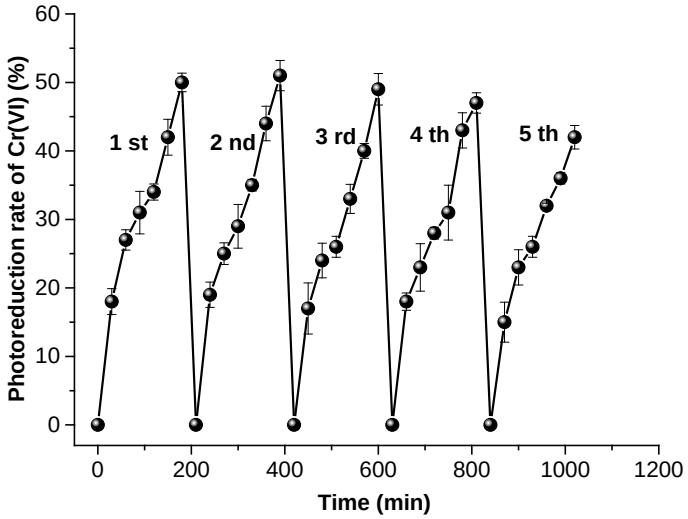
Photoreduction rate of Cr(VI) (%)
Time (min)
1 st
2 nd
3 rd
4 th
5 th
0
10
20
30
40
50
60
0
200
400
600
800
1000
1200